Romanian Reports in Physics, Vol. 57, No. 4, P. 715–746, 2005

ESTIMATES OF ALPHA-DECAY HALF-LIVES OF SUPERHEAVY ELEMENTS

I. SILIȘTEANU[1], W. SCHEID[2] AND A. O. SILIȘTEANU[1]

[1] *Institute of Atomic Physics, Bucharest-Măgurele, Romania*
[2] *Institut für Theoretische Physik der Justus-Liebig-Universität, Giessen, Germany*

(Received September 9, 2005)

Abstract. The main conceptual issues in reaction decay theory are identified and their relative importance is assessed: these include, couplings between the relative motion of the fragments and several nuclear collective motions, the existence and convergence of the resonance scattering solution, account the effects of non-linear couplings to all orders, self-consistence of the scattering potential, and the rotational excitation of nuclei by the cluster transfer. A brief outlook of the experimental results and theoretical ideas which define the clustering, tunneling and "fine structure" is presented together with quantitative estimations for resonance decay widths. We present both formal considerations, derived from a microscopic (shell model) formulation of the reaction theory, and practical computational programs based on coupled channel methods, with many-body effects included in formation and reaction amplitudes, energy shifts and total decay widths. The cluster decay properties of nuclei are considered and some spectroscopic informations on the continuum states populated in in the unbound intermediate systems in the decay channel are obtained. The advantages and limitations of current approaches are addressed, with particular regard to quantitative experimental comparisons for superheavy nuclei.

Key words: nucleon clustering, quantum tunneling, "fine structure", reaction dynamics, multichannel emission, channel coupling, resonant particle spectroscopy.

PACS numbers: 25.70.Jj; 27.90.+b

1. INTRODUCTION

In this paper we apply the basis many-particle wave functions for clustering and fine structure (FS) to the time independent Schrodinger type equations, written in the form of projection equations, to formulate a unified microscopic nuclear structure and reaction theory for the multichannel cluster decay. In resulting approach we treat the nuclear cluster decay from the nuclear reaction point of view as a resonance reaction and represent the single channel and multichannel decay rates by means of simple resonance formulas. The problems considered below may help for the understanding of the present status of reaction decay theory and of essential computer codes that implement this theory.

In most cases the objectives and subjects of the nuclear decay theory have been to make use of measurements and observations on nuclear reactions in order to derive conclusions concerning nuclear properties. This involves developing and applying theories and methods of predictions, analysis and interpretation of experiments, with the aim of achieving a deeper understanding of the physical nature of quantal many body systems. The success of modern theory represents one of the few cases in which considerable theoretical efforts have explicitly focused on quantitative treatment of new experimental techniques and methods and shows what can be achieved with such a focus. Current research topics in field include production of radioactive nuclei at the limits of stability, decay and in-beam studies, properties and probes of nuclear matter at limits, macroscopic static and dynamic nuclear properties and microscopic simulations.

It is only during the last several years that the limit of nuclear stability has been reached in few areas of nuclide chart. Exploration of new regions of the nuclear chart is expected to reveal nuclei with unusual sizes, shapes, and new decay modes. There is widespread interest in p, $2p$, α, and heavy cluster (HC) emission near the proton drip-line, and both prompt and delayed β. As nuclei move further from β stability on the proton rich side, their binding energy rapidly decreases, due to increasing Coulombic repulsion and reaction Q-values, which leads to two major difficulties in their studies. One is related to the reaction mechanism for their production and the other to their nuclear decay properties. The relatively large Q-values cause high excitations in nuclear systems involved and open up many competing reaction channels favoring the nuclei closer to stability. Damping these excitation can be very crucial for radioactive nuclei produced near the limit of proton stability, because their ground states are often the only bound states. Another difficulty is related to the study of nuclear decay properties. Depending on the experimental approach in production of radioactive nuclei, our bijective in this paper is the determination of a nuclide's "existence" or particle (cluster) stability, its main decay modes and half-life, its ground state mass, or its excited states and their decay.

Clustering and FS are two of most important typical structures (TS) in nuclear physics strongly connected with the shapes, deformation and stability of nuclei. The experimental signatures of these structures have been traditionally strong for radioactive nuclei and are supported by selective excitation in nucleon and α-decay and α-transfer reactions, heavy cluster decay, and by rotational and vibrational spaced energy levels, enhanced transition strengths and intensities, and appreciable emission width for the resonant states above the decay theshold. Recent decay and in-beam studies of nuclei far from stability are revealing an unexpected diversity and richness of shapes, new decay modes and TS which are related to very low binding energy and the strong influence of the continuum.

Spectroscopic studies of nuclei close to proton drip-line are particularly interesting. First, because the structure of these nuclei differs strongly from that of

other nuclei, they can have an unusual spectrum of energy levels. Second, the lover levels of these nuclei are inevitably near the proton emission tresholds and the proton and α-decay channels are effectively, the only open ones. Third, spectroscopic studies of long chains of isotopes extending far of stability, make possible to access the basic nuclear-ground state properties of new EN or SHE: their masses, lifetimes, energy levels, spins, moments, and sizes. Thus, observation and measurements of the TS in α-decay may provide a powerful method to extend the energy and spin-parity informations from daughter to parent with support from theoretical investigations and this may lead to identification of nuclei in long decay chains and determining the excitation energies of the daughter nucleus from decay and in-beam studies. Progress in obtaining the most complete information on the development of TS from stable to exotic losely-bound nuclei and from lightest to heaviest nuclei is being made on several fronts: 1) improving the structure models in order to describe essential features and obtain spectroscopic information on a number of nuclei that can then tested against data extracted from decay and in-beam studies; 2) extending the range of applicability of reaction models by using accurate reaction channels methods (*e.g.*, *via* additional channels including deformation, exchange effects, antysimmetrisation, etc); 3) including microscopic structure information in coupled channel reaction models and treating more carefully of "intermediate" systems that are more or less bound or have mixed composition.

In Section 2 we present the basic formulas for calculating the emission rates in the single channel and many channel cases. In Section 2.1 we stress some of the resonance features of the single channel solution that we shall require for the extension, in Section 2.2 to the resonance solution in many channel case. The resonance solution of systems of coupled equations is obtained by a direct numerical integration using step-by-step methods on computer. Some variants of the Gordon and Numerow methods are found to be most efficient for all these problems. Applications are given in Sections 3–6. Section 4 compares the our results with the previous ones and data and recent data. Concluding remarks are made in Section 7.

2. AN OUTLINE OF THE THEORY

The first microscopic description of α-decay was an application of of a general theory of nuclear reactions, the R-matrix theory [1, 2]. This, combined with shell model, which was introduced at the same time, opened the possibility of performing microscopic calculations for the nucleon clustering into the α-particle and its subsequent emission [3, 4, 5]. The *R*-matrix width contains the channel radius parameter, which is an arbitrary parameter and often is interpreted as disavantage of the theory. To overcome this disavantage, in the dynamical reaction

theories [6, 7] have been formulated alternative approximations [8–13] which are reviewed in [14]. The dominant feature of many reaction processes in which two nuclei collide at low energies to form a compound nucleus, which subsequently disintegrates in a pair of nuclei, is the appearance of resonances [15–17]. The characteristic common to all these approximations is the employments of quasi-stationary resonance levels and the competition between the different modes of disintegrations. The experimental observation of resonances has a great importance in reaction with heavy ions since when they are sharp they may be interpreted as levels of reaction product and since such connection contributes directly to decay and in-beam studies of nuclear structure. In many cases the experimental result is usually clear to indicate the position of level and his width to derive some conclusion regarding the size of system or the internal normalization of the wave function if it is adjusted to give unit flux at an infinite distance.

From a mathematical point of view, the problems of Gamow states defined as eigenstates of the time independent Schrödinger equation with purely outgoing boundary, are very similar to those of the continuum shell model for nucleons [15]. In the both cases, the usual quantum mechanical rules for normalizations, orthogonality and completeness have to be extended in order to take into account the bound as well as scattering wave functions in a straightforward manner. The complex eigenvalue solutions of the Schrödinger equation give the positions of the resonance states as well as their lifetimes. A description of the resonance phenomena *via* complex eigenvalue solutions has the advantage of containing stationary structures as well as dynamic coupling effects.

It is the aim of the present paper to extend the developments [12, 17–19] in order to study the radioactive decay properties of nuclei at the limits of stability.

2.1. SINGLE CHANNEL. SPHERICAL SYSTEM

In the simplest case of decay of a single resonance state k into a single decay channel n, the α-decay width obtained in [12] as well as the heavy cluster decay width [19] is:

$$\Gamma_n^k = 2\pi \left| \frac{\int_{r_{\min}}^{r_{\max}} I_n^k(r) u_n^0(r) \mathrm{d}r}{\int_{r_{\min}}^{r_{\max}} I_n^k(r) u_n^k(r) \mathrm{d}r} \right|^2 \tag{1}$$

where $I_n^{\nu}(r)$ is the particle (cluster) formation amplitude (FA) and $u_n^k(r)$ and $u_n^0(r)$ are the solutions of the system of differential equations

$$\left[\frac{\hbar^2}{2m} \frac{\mathrm{d}^2}{\mathrm{d}r^2} - V_n(r) + Q_n \right] u_n^0(r) = 0 \tag{2}$$

$$\left[\frac{\hbar^2}{2m}\frac{\mathrm{d}^2}{\mathrm{d}r^2} - V_n(r) + Q_n\right] u_n^k(r) = I_n^k(r). \tag{3}$$

The radial functions in Eqs. (2) and (3) describe the radial motion of the fragments at large and small separations, respectively by using the reduced mass m, the kinetic energy of emitted particle $Q_n = E - E_D - E_p$, the FA $I_n^k(r)$, and the interaction potential $V(r)$.

The FA is the antisymmetrized projection of the parent wave function (WF) $|\Psi_k\rangle$ on the channel WF $|n\rangle = \left|\left[\Phi_D(\eta_1)\Phi_p(\eta_2)Y_{lm}(\hat{r})\right]_n\right\rangle$:

$$I_n^k(r) = r\left\langle \Psi_k \middle| \mathcal{A}\left\{\left[\Phi_D(\eta_1)\Phi_p(\eta_2)Y_{lm}(\hat{r})\right]_n\right\}\right\rangle \tag{4}$$

where $\Phi_1(\eta_1)$ and $\Phi_2(\eta_2)$ are the internal (space-spin) wave functions of the fragments, $Y_{lm}(\hat{r})$ is the wave function of the angular motion, $\mathcal{A}$ is the inter-fragment antisymmetrizer, r connects the centres of mass of the fragments, and the symbol $\langle|\rangle$ means integration over the internal coordinates and angular coordinates of relative motion. The potential is given by the matrix element of the nuclear, Coulomb, spin-orbit and centrifugal parts:

$$V_n(r) = \langle n\left| \left[V^{nucl.}(r) + V^{Coul.}(r) + V^{so}(r) + \frac{\hbar^2}{2m}\frac{l(l+1)}{r^2}\right]\right| n\rangle, \tag{5}$$

The parametrisation of these parts of the interaction is detailed in Appendix.

The equations (2, 3) are solved with usual boundary conditions for the decay problem:

$$u_n^0(r \to 0) = 0 \tag{6}$$

$$u_n^0(r \to \infty) \to i/2(k_n/\pi Q_n)^{1/2}\{u_n^{(-)}(r) + S_n u_n^{(+)}\} \tag{7}$$

$$u_n^{\nu}(r \to 0) = 0 \tag{8}$$

$$u_n^{\nu}(r \to \infty) = 0 \tag{9}$$

where $\hbar k_n = (2mQ_n)^{1/2}$, S_n is the scattering matrix, $u_n^{(\pm)}(r) = G_n(r) \pm iF_n(r)$ and F_n and G_n are the regular and irregular Coulomb functions. In spherical systems the s.p. angular momentum is conserved and and the scattering martix is diagonal in the angular momentum representation.

To avoid the usual ambiguities encountered in formulating the potential for the resonance tunnelling of the spherical barrier we iterate directly the nuclear potential in equations of motion.

Since Eq. (2) is linear and homogeneous any solution with the correct behavior at the origin will be a multiple of any other solution with the same initial condition. Thus the second point in the solution may be chosen completely arbitrarily and the overall normalization determined by matching to the required form in the asymptotic region.

For the lower limit in integrals (1) we choose an arbitrary small radius $r_{\min} > 0$. The upper limit $r_{\max}$ is close to the first exterior node of $u_n^0(r)$ since this function decreases rapidly with *r* after the barrier and is essentially confined in the interval $\left[r_{\min}, r_{\max}\right]$.

2.2. COUPLED CHANNELS. DEFORMED SYSTEM

Our aim in this paper is to generalize the microscopic approximation [12] for the many channel case. Based on the existing data, including the nuclear deformations, relvant interactions between decay products and realistic nuclear radii we have constructed the decay schemes which imply the excitation of the rotational degree of freedom in radioactive decay. To treat the decay rates for emitted particles groups with similar energies we must to describe the nuclear clustering and penetration of the particle through the potential barrier taking into account the correspondence between different decay channels and different final states of the daughter nucleus. The usual way to address the effects of coupling between the intrinsic degrees of freedom and relative motion is to numerically solve the coupled channel equations, including all the relevant channels [20]. Thus, the total decay width for the multichannel decay of the state k into a set of $\{n\}$ different channels is given by (see Appendix):

$$\Gamma^k = 2\pi_n \sum_n \Gamma_n^k = 2\pi \sum_n \left| \frac{\int_{r_{\min}}^{r_{\max}} I_n^k(r) u_n^0(r) \mathrm{d}r}{\int_{r_{\min}}^{r_{\max}} I_n^k(r) u_n^k(r) \mathrm{d}r} \right|^2 \tag{10}$$

i.e. the sum of the partial decay widths:

$$\Gamma_n^k = 2\pi \left| \frac{\int_{r_{\min}}^{r_{\max}} I_n^k(r) u_n^0(r) \mathrm{d}r}{\int_{r_{\min}}^{r_{\max}} I_n^k(r) u_n^k(r) \mathrm{d}r} \right|^2 . \tag{11}$$

In Eq. () $I_n^v(r)$ is the particle (cluster) formation amplitude (FA) and $u_n^k(r)$ and $u_n^0(r)$ are the solutions of the systems of differential equations

$$\left[\frac{\hbar^2}{2m}\left(\frac{\mathrm{d}^2}{\mathrm{d}r^2}-\frac{l(l+1)}{r^2}\right)-V_{nn}(r)+Q_n\right]u_n^0(r)+\sum_{m\neq n}V_{nm}(r)u_m^0(r)=0 \qquad (12)$$

$$\left[\frac{\hbar^2}{2m}\left(\frac{\mathrm{d}^2}{\mathrm{d}r^2}-\frac{l(l+1)}{r^2}\right)-V_{nn}(r)+Q_n\right]u_n^{\nu}(r)+\sum_{m\neq n}V_{nm}(r)u_m^{\nu}(r)=I_n^{\nu}(r) \qquad (13)$$

The radial functions in the system of equations Eqs.( ) and (3) describe the radial motion of the fragments at large and small separations, respectively, by using the reduced mass m, the kinetic energy of emitted particle groups $Q_n = E - E_D - E_p$, the FAs $I_n^k(r)$, and the matrix elements $V_{nm}(r)$ of the interaction potential.

The FA is obtained as an antisymmetrized projection of the parent wave function (WF) $|\Psi_k\rangle$ on the channel WF $|n\rangle = \left|\left[\Phi_D(\eta_1)\Phi_p(\eta_2)Y_{lm}(\hat{r})\right]_n\right\rangle$:

$$I_n^k(r) = r\langle\Psi_k|\mathcal{A}|n\rangle = r\left\langle\Psi_k\left|\mathcal{A}\left\{\left[\Phi_D(\eta_1)\Phi_p(\eta_2)Y_{lm}(\hat{r})\right]_n\right\}\right\rangle. \qquad (14)$$

The FA depends on the radial distance between the fragments and also on nuclear deformations of involved nuclei. The matrix elements of the interaction potential are given by:

$$V_{nn}(r) = \langle n|V^{nucl.}(r) + V^{Coul.}(r) + V^{so}(r)|n\rangle \quad \text{and} \qquad (15)$$

$$V_{nm}(r) = \langle n|V^{nucl.}(r) + V^{Coul.}(r) + V^{so}(r)|m\rangle \qquad (16)$$

In the case in which all exit channels are open the boundary conditions should be:

$$u_n^0(r\to 0) = 0, \qquad (17)$$

$$u_n^0(r\to\infty) \to i/2(k_n/\pi Q_n)^{1/2}\left\{\delta_{nm}\exp\left[-i(k_n - l\pi/2)\right] - S_{nm}\exp\left[i(k_n r - l\pi/2)\right]\right\} \qquad (18)$$

$$u_n^{\nu}(r\to 0) = 0, \qquad (19)$$

$$u_n^{\nu}(r\to\infty) = 0 \qquad (20)$$

where S_{nm} is the scattering matrix. If the matrix elements of the interaction potential have no singularities of order two or higher at the origin, then for small the solutions of (9) with that satisfy (11) are given by $u_n^0(r) = a_n r^{l+1}$ where a is a matrix of constants. The solutions thus obtained will not, in general, satisfy the asymptotic boundary conditions (17–20). Thus, N linearly independent solutions of (12) must be found and a suitable linear combination of them matched to the correct asymptotic form. The solutions $u_n^0(r)$ may be matched to the boundary conditions

at two values of r large enough so the terms V_{nm} are negligible (see Appendix). A special type of eigenvalue solution will be considered here for which the behavior of solution in each separate channel is similar to that of G_n in the one channel problem. In each channel the absolute value of $u_n^0(r)$ decreases to the of small fraction of its value inside of nucleus and only after that enters the region within which it has an oscillatory character (the condition being similar to that of resonances in the central field). Such a solution can be modified by introduction of potential barrier extending to large in order to convert the decaying state into a discrete level with a single decay channel. The solution inside the nucleus can be expected to be unaffected by the removal of the barriers and its amplitude to decreases approximately with the time as in the case of one channel problem. To avoid the usual ambiguities encountered in formulating the potential for the resonance tunnelling of the deformed barrier we iterate directly the nuclear potential in equations of motion (12–13).

The "one-body" (o.b.) resonance width in the many channel problem can be expressed only with the eigenvalues and eigenfunctions of the system:

$$\Gamma_n^{o.b.} = 2\pi \left| \frac{\int_{r_{\min}}^{r_{\max}} G_n(r) u_n^0(r) \mathrm{d}r}{\int_{r_{\min}}^{r_{\max}} G_n(r) u_n^{o.b.}(r) \mathrm{d}r} \right|^2 . \tag{21}$$

where $u_l^{o.b.}(r)$ is a solution of Eq. (13) in which $I_n^k(r)$ is merely replaced by $G_n(r)$.

The decay width formulas (1, 7, 15) are not dependent on an arbitrary radius such as the channel radius or other energy dependent parameters of theory. In form the result (7) is like the one known in the Wigner R-matrix theory $\Gamma_n = \gamma_n^2(r = R_c) P_n(r = R_c)$. While this width is estimated at a somewhat arbitrary channel radius R_c such a radius is not necessary in our approach.

The basic step necessary for the determination of the emission rates is the calculation of FA and also RA by integrating the equations of motion. We obtain the partial resonance widths for all the open decay channels and also a model independent determination of resonance emission energies as eigenenergies of the system. The calculated widths and emission energies can be directly confronted to the decay data.

3. MODELS FOR α-DECAY PROPERTIES

Theoretical models for α-decay properties have evoluated from macroscopic-microscopic models such as the finite droplet model with shell corrections [21–24],

to fully microscopic deformed Hartree Foock (HF) model [14, 15], mean field models [25–26] or phenomenological model [27, 28]. In addition to their importance for for many-body nuclear structure, theoretical models for the prediction of the decay properties are very important when designing experiments since the techniques used will depend on the half-life and decay mode. The role and importance of configuration mixing [29], exchange effects [30], two and four particle [31–32] correlations and nuclear deformation [33] have been more or less clarified. There is now an intense work on the theoretical aspects of the α-decay and heavy cluster decay problems. The rapid developments of the computing facilities has made it possible extensive calculations on the old but still largely open problems of the micoscopic decay theory.

4. EXPERIMENTAL DECAY STUDIES

Synthesis and study of new radioactive nuclei need to perform experiments in reasonable measuring times and a large number of investigations covering reaction physics at Coulomb energies and also the emission spectroscopy. With the multistrip and position-sensitive charged-particle detectors, new experimental methods become available for studying the typical structures in nuclei: the resonant particle spectroscopy (RPS) [34–35], and the so called recoil decay tagging (RDT) method [36]. These methods involve the coincidence detection of the decay products of highly excited nuclei, wich permits a measurement of partial rates for different decay channels. In such measurements the resonant particle may be excited via transfer reactions or inelastic scattering. Using these methods, very weak reaction channels can be studied by requiring a coincidence between prompt gamma-rays from the target and fusion products in the focal plane of a recoil separator and identified on the basis of their characteristic decay. Thus, an improved technique for gas-phase experiments coupled on-line to a versatile detection system for α-decay chains has been developed was made possible to detect the new α-decaying transactinides, through their characteristic α-decay and preferably by observed $\alpha\alpha$-mother-daughter correlations [37–45]. Since, α-decay chain provides very clear signatures of the nuclides from the beginning of the decay chain, the decay chain can be reconstructed from the bottom, and therefore, it is possible to identify the initial parent through measured α-α (parent-daughter) correlations in the chain. Therefore, our procedures for α-decay rates based on the analysis of reaction dynamics and emission spectroscopy may be useful to design the RPS and RDT methods in future experiments for SHEs.

New experimental facilities have opened the possibility of getting information on the nuclear deformation through the study of α-decay. Since in most cases far from stability nuclei are well deformed, this makes possible the observation of

several emitted particle groups with similar energies. In fact, this may reveal important information on nuclear structure and provide in many cases a powerful method of extending the energy-spin-parity information from daughter nuclide to the parent. Observation and study of the clustering and fine structure in α-decay may provide also a method of determining the excitation energies of the daughter nucleus. From the analysis of α-decay data, it is also possible to deduce with solid theoretical support the information on s.p. states in SHE. It would be of great importance to learn about single particle states in SHE *via* decay and in beam studies of the odd-mass nuclei.

Experimentally, there is a clear evidence for clustering and fine structure in SHE. The capabilities for investigating these typical structures in SHE have been extended by the development of the techniques of resonant-particle spectroscopy and the employment of the recoil decay tagging method in connection to in-beam measurements. More detailed spectroscopic measurements will be required to understand typical structures in SHE.

5. α-HALF-LIFE ESTIMATES

The α-half-time is calculated from Eqs. (1, 10) in which the emission energy is given by the measured Q_α-value (if this is available) or calculated value (O^*_α, see Tables) in case of "escape" α-particle. Since, the channel wave functions and formation amplitudes are provided by the single-particle models for reaction dynamics and nuclear structure, we use these models to estimate the formation and reaction probabilities, emission energies for "escape" particles and finally the halftime. The heaviest known elements were all identified from their α-decay chains, because α-decay chains provide very clear signatures of the nuclear species in the beginning of the decay chain whereas fission does not, it is of major interest to estimate accurately the α-decay properties of these nuclei.

5.1. THE ELEMENT 110

The α-decay measurements [37] of four decay chains assigned to $^{269}110$ are presented in Table 1 and Fig. 1. The first chain starts with an emission energy of 11.132 ± 0.020 MeV and a time interval t (between two successive α-events of the chain) of 393 μs after an implantation signal of 25 MeV. The calculated half-time T for the ground state emission at this energy is 300 μ*s*.

In Fig. 1 (left) we represent log$t$ *versus* $Q_\alpha^{-1/2}$. One can see that, the log$t$ increases with decreasing energy. A small deviation of log$t$ from this trend can be seen only at the beginning of channel 3. In such a plot the chain events appear time

Table 1

Summary of the α-decay data and calculated α-decay half-lives for $^{269}110$ and its α-descendants. The calculated Q_α-values for α-particles are marked by (*). The decay chain assignments have been obtained in experiments at GSI-Darmstadt (Hofmann *et al.* [37]) using the reaction of $^{62}Ni + {}^{208}Pb \rightarrow {}^{269}110 + 1n$. The time $t = t_1 - t_2$ denotes the time separation between two successive events of the chain

Alpha chain	Parent nucleus	Q_α [MeV]	$t = t_1 - t_2$ [s] Experiment	T [s] Estimation
$I - \alpha_1$	$^{269}110$	11.132	$0.353 \cdot 10^{-3}$	$0.300 \cdot 10^{-3}$
$I - \alpha_2$	$^{265}108$	10.574	$0.583 \cdot 10^{-3}$	$0.176 \cdot 10^{-2}$
$I - \alpha_3$	$^{261}106$	9.576	$0.720 \cdot 10^{-1}$	0.141
$I - \alpha_4$	$^{257}104$	9.075*	0.779	0.815
$II - \alpha_1$	$^{269}110$	11.208 *	$0.201 \cdot 10^{-3}$	$0.178 \cdot 10^{-3}$
$II - \alpha_2$	$^{265}108$	10.574	$0.203 \cdot 10^{-2}$	$0.209 \cdot 10^{-2}$
$II - \alpha_3$	$^{261}106$	9.524	0.373	0.235
$III - \alpha_1$	$^{269}110$	11.095	$0.142 \cdot 10^{-3}$	$0.366 \cdot 10^{-3}$
$III - \alpha_2$	$^{265}108$	10.519	$0.126 \cdot 10^{-3}$	$0.228 \cdot 10^{-2}$
$III - \alpha_3$	$^{261}106$	9.554	0.155	0.193
$III - \alpha_4$	$^{257}104$	8.705	$0.261 \cdot 10^{+2}$	$0.148 \cdot 10^{+2}$
$III - \alpha_5$	$^{253}102$	8.144	$0.224 \cdot 10^{+3}$	$0.217 \cdot 10^{+3}$
$IV - \alpha_1$	$^{269}110$	11.110	$0.241 \cdot 10^{-3}$	$0.338 \cdot 10^{-3}$
$IV - \alpha_2$	$^{265}108$	10.571	$0.232 \cdot 10^{-2}$	$0.170 \cdot 10^{-2}$
$IV - \alpha_3$	$^{261}106$	9.468	$0.340 \cdot 10^{+1}$	0.339
$IV - \alpha_4$	$^{257}104$	8.615	$0.139 \cdot 10^{+2}$	$0.291 \cdot 10^{+2}$
$IV - \alpha_5$	$^{253}102$	8.022	$0.427 \cdot 10^{+3}$	$0.586 \cdot 10^{+3}$

ordered with respect to emission energy. The experimental half-life of the nuclide $^{269}110$ has been determined in [1] by averaging the measured times t for all competing channels.

The Fig. 1 shows in a Gamow plot the estimated half-lives T. In this plot one may observe that the chain events follow exactly in order of the energy decrease, so that a simple rule results: the shortest half-life always corresponds to the highest energy. The result of global fit of estimated half-lives (with the Gamow formula: $logT = AQ_\alpha^{-1/2} + B$, A and B being the constants for the slope and structure, respectively) is also shown by dot line. In Fig. 1 one may see relatively small single event deviations from the Gamow line ($A = 131.438$, $B = -38.466$). Three distinct groups of α-particles of rather different emission energies can be seen in the case of the nuclides $^{269}110$, $^{265}108$ and $^{261}106$. Moreover, the excitation energies of successive daughters seem to increase far from the magic shells ($Z = 114$, $N = 184$).

Calculations for $N = 162$ and $Z = 108$–110 [46] indicate the bunching of levels with spin and parities $1/2^+$, $3/2^+$, $7/2^+$, $9/2^+$ and $11/2^-$ and also the large gap of about 1 MeV up the next higher level. This complicated pattern can lead to energetically close lying isomeric states. α-transitions of similar half-lives between these states can occur due to the fact that energies are comparable. Microscopic analysis of one-quasiparticle neutron states, α-decay energies and deformations has been performed in [24]. Unfortunately, a definitive assignment of the decay channels to the ground states or excited levels of odd-*A* nuclei is not possible on the basis of data now available.

5.2. THE ELEMENT 111

The decay data [38] and present half-time estimates to the α-decay of $^{272}111$ and its descendants are included in Table 2 and Fig. 1 (bottom). Notice in Fig. 1 that, log*t* and log*T* *versus* $Q_\alpha^{-1/2}$ show similar trends as in the case of $^{269}110$ nuclide. The resulting Gamow constants for $^{272}111$ ($A = 100.309$, $B = -32.993$) differ significantly from those of $^{269}110$. Here, it should be stressed the quality of data obtained in experiment [38].

Table 2

Same as in Table 1, but for $^{272}111$. The decay chains and assignments have been obtained in experiments at GSI-Darmstadt (Hofmann *et al.* [38]) using the reaction of $^{64}Ni + {}^{209}Bi \rightarrow {}^{272}111 + 11n$.

Alpha chain	Parent nucleus	Q_α [MeV]	$t = t_1 - t_2$ [s] Experiment	T [s] Estimation
I - α_1	$^{272}111$	10.750*	$0.360\cdot10^{-2}$	$0.375\cdot10^{-2}$
I - α_2	$^{268}109$	10.259	$0.710\cdot10^{-1}$	$0.452\cdot10^{-1}$ (l = 3)
				$0.157\cdot10^{-1}$ (l = 0)
I - α_3	$^{264}107$	9.475	$0.980\cdot10^{-1}$	0.519
I - α_4	$^{260}105$	9.058*	$0.196\cdot10^{+1}$	$0.206\cdot10^{+1}$
II - α_1	$^{272}111$	11.047*	$0.696\cdot10^{-3}$	$0.899\cdot10^{-3}$
II - α_2	$^{268}109$	10.097	0.171	0.041
II - α_3	$^{264}107$	9.618	0.334	0.230
II - α_4	$^{260}105$	9.146	0.953	$0.106\cdot10^{+1}$
III - α_1	$^{272}111$	10.820	$0.204\cdot10^{-2}$	$0.241\cdot10^{-2}$
III - α_2	$^{268}109$	10.221	$0.720\cdot10^{-1}$	$0.556\cdot10^{-1}$ (l = 3)
				$0.197\cdot10^{-1}$ (l = 0)
III - α_3	$^{264}107$	9.621	$0.145\cdot10^{+1}$	0.200
III - α_4	$^{260}105$	9.200	0.573	0.734
III - α_4	$^{256}103$	8.463	$0.665\cdot10^{+2}$	$0.311\cdot10^{+2}$

5.3. THE ELEMENT 112

The decay data [39] assigned to the nuclide $^{277}112$ and its α-descendants and our half-time estimates for all these nuclides are presented in Table 3 and Fig. 1 (left). In this case the obtained Gamow constants are $A = 131.628$ and $B = -32.993$, respectively. The decay data show interesting features:

i) The two channels reveal two very different decay properties of daughter $^{273}110$ with $Q_\alpha = 11.08$ MeV, $t = 76$ μs (chain 2) and $Q_\alpha = 9.73$ MeV, $t = 120$ ms (chain 1). Thus, a state of daughter nucleus appears at the unexpected higher excitation energy of 1.35 MeV. These large differences are due to spin isomerism or if shape isomerism is responsible.

ii) Fig. 1 shows large deviations of log$t$ from its general trend to increase with the energy decrease. Furthermore, even for the parent case log$t$ decreases with the energy decrease. Notice that, possible errors in the position and time measurements and the inadequate position calibrations for energies far off the full energy α-lines may lead to an apparent "inversion " for time t as a function of energy.

iii) The measured times t and energies for two distinct channels (states) of the daughter nuclide $^{273}110$ are very close to the ones of parent nuclide $^{277}112$. Similar times and energies show $^{269}108$ and $^{265}106$. These similarities lead to additional difficulties in assignments of data.

Table 3

Same as in Table 1, but for $^{277}112$. The decay chains and assignments have been obtained in experiments at GSI-Darmstadt (Hofmann *et al.* [39]) using the reaction $^{70}Zn + {}^{208}Pb \rightarrow {}^{277}112 + 1n$

Alpha chain	Parent nucleus	Q_α [MeV]	$\tau = t_1 - t_2$ [s] Experiment	T_α [s] Estimation
$I - \alpha_1$	$^{277}112$	11.65	$0.40\cdot10^{-3}$	$0.59\cdot10^{-4}$
$I - \alpha_2$	$^{273}110$	9.73	0.17	0.80
$I - \alpha_3$	$^{269}108$	9.17	7.10	9.09
$I - \alpha_4$	$^{265}106$	8.77	24.10	34.40
$I - \alpha_5$	$^{261}104$	8.56*	32.70	37.83
$II - \alpha_1$	$^{277}112$	11.45	$0.28\cdot10^{-3}$	$0.16\cdot10^{-3}$
$II - \alpha_2$	$^{273}110$	11.08	$0.11\cdot10^{-3}$	$0.31\cdot10^{-3}$
$II - \alpha_3$	$^{269}108$	9.23	19.70	6.03
$II - \alpha_4$	$^{265}106$	8.98	7.40	7.13
$II - \alpha_5$	$^{261}104$	8.52	4.70	45.11
$II - \alpha_6$	$^{257}102$	8.34	15.00	35.01
$III - \alpha_1$	$^{277}112$	11.17	$0.14\cdot10^{-4}$	$0.72\cdot10^{-3}$
$III - \alpha_2$	$^{273}110$	11.20	$0.31\cdot10^{-3}$	$0.32\cdot10^{-3}$
$III - \alpha_3$	$^{269}108$	9.18	22.00	8.47
$III - \alpha_4$	$^{265}106$	8.85*	18.80	18.14

In order to clarify some points of the experiment [3] a more complete excitation-function systematic for production of element 112 isotopes would be highly desirable. Our results are different from empirical ones obtained by using old procedures based on Viola-Seaborg formula of parameters fitted in the HE region for two reasons. First, we now use experimental Q_α-values obtained recently. Second, Figs. 1 and 2 show that half lives of different SHE can be fitted accurately with rather different Gamow constants. Therefore, the use of the same fit constants for all SHE is expected to introduce large errors in some half-lives predicted empirically. The unambiguous identification of heaviest elements with $Z = 110$–112 [37–39] has been essentially based on the connection of observed decay sequences to below nuclides safely identified before.

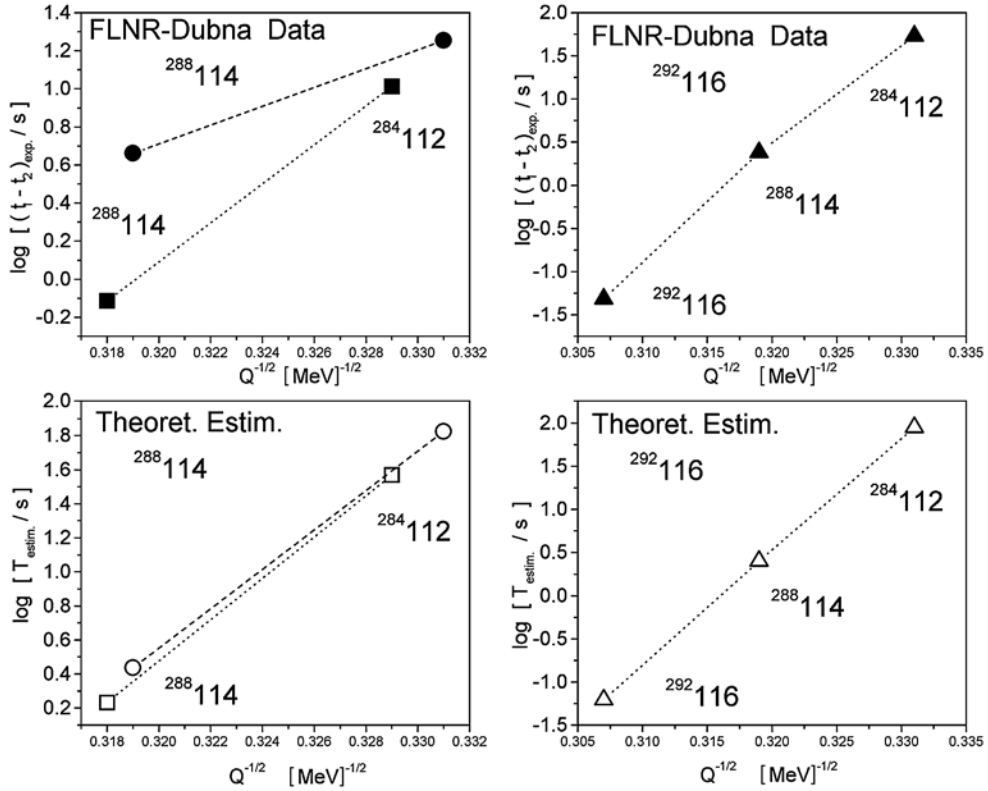

Fig. 2 – Summary of the α-decay data obtained by Oganessian *et al.* [40–42] for $^{287–289}$114 isotopes and estimated α-half-lives.

5.4. THE ELEMENT 114

In reactions of ^{242,244}Pu with ^{48}Ca ions [40–43] a chain of decay has been detected which matched very well the signature expected for the decay of a SHE 114 .

Table 4

Same as in Table 1. but for $^{287-289}114$. The decay chains and assignments have been obtained from experiments at FLNR-Dubna (Oganessian *et al.* [40]) using the reaction $^{48}Ca + + ^{242,244}Pu \rightarrow \rightarrow ^{287-289}114 + 2n(3n, 4n)$

Alpha chain	Parent nucleus	Q_α [MeV]	$t = t_1 - t_2$ [s] Experim.	T [s] Theoret.	T [s] Empirical
$I - \alpha_1$	$^{287}114$	10.29	1.32	1.21	
$II - \alpha_1$	$^{287}114$	9.90*	14.40	15.34	
$I - \alpha_1$	$^{287}114$	9.87	0.77	2.20	1
$I - \alpha_2$	$^{284}112$	9.21	10.03	10.71	4
$II - \alpha_1$	$^{288}114$	9.80	4.60	3.50	1
$II - \alpha_2$	$^{284}112$	9.13	18.00	65.59	4
$I - \alpha_1$	$^{289}114$	9.71	30.4	31.8	2–23
$I - \alpha_2$	$^{285}112$	8.67	924	14 900	1200–12000
$I - \alpha_3$	$^{281}110$	8.83	96	840	60–720

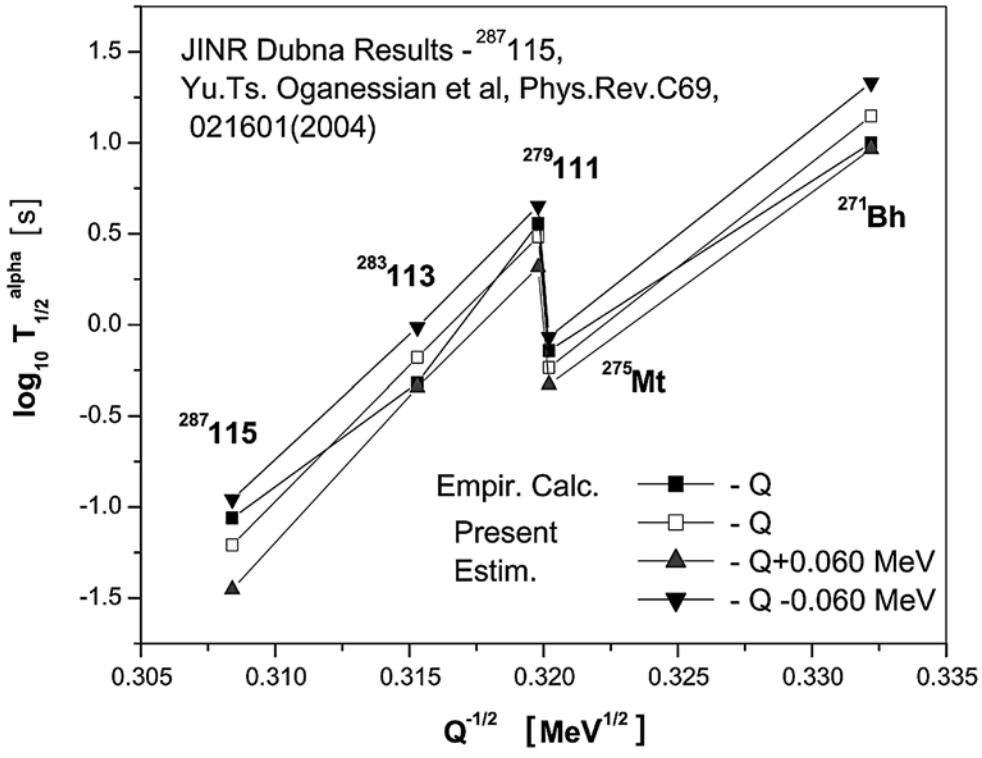

Fig. 3 – The Gamow plot for experimental [44] and estimated α-half-lives for the decay chain of $^{287}115$.

The excited energy of the compound nucleus $^{292}114$ has been limited to about 32–35 MeV at bombarding energies near the Coulomb barrier. This seems to offer a much greater survival probability than hot fusion reactions which may produce the excitation energies of about 45–50 MeV at the barrier. For such excitation energies the compound nucleus is expected to evaporate 2 to 4 neutrons, most likely 3. This would result in the final evaporation residues being $^{287–289}114$. The results of these experiments are included in Table 4 and Fig. 3. Due to missing implantation signals some experimental times t could not be obtained. An escape α-particle exists even for $^{287}114$ nuclide. The value $Q_\alpha = 8.83$ MeV of $^{281}110$ is greater than the one of its parent $^{285}112$ of $Q_\alpha = 8.67$ MeV. This denotes an inversion from the general trend of log$T$ with the energy decrease. Fig. 2 shows two quite different Gamow lines for odd and even N nuclides from the chains of 114 element. From Table 4 notice that the present estimations reasonably agree with the empirical ones [40–42].

5.5. THE ELEMENT 115

The results of experiments designed to synthetisize element 115 isotopes in the $^{243}Am + {}^{48}Ca$ have been presented in [44]. For the odd Z elements, especially for their odd-odd isotopes, the probability of α-decay with respect to SF should increase due to hindrance for SF. For such nuclei one might expect longer consecutive α-decay chains terminated by SFf relatively light descendant nuclides with $Z \leq 105$. The observation of nuclei passing from spherical to deformed shapes in the course of their consecutive α-decays could provide valuable information about the influence of significant structure changes on the nuclear decay properties properties of SHE with $Z = 114–118$ obtained in ^{48}Ca-induced reactions with actinide targets ^{244}Pu, ^{248}Cm, ^{249}Cf.

5.6. THE ELEMENT 116

The experiment [45] was designed to investigate the radioactive properties of the isotopes of element 116, the α-decay daughters of $Z = 118$ isotopes produced in the reaction $^{249}Cf + {}^{48}Ca$. In this reaction have been synthetsized two new isotopes of element 116 that undergo sequential α decays terminated by spontaneous fission. The α particle spectra observed in these experiments are characterized by well-defined transition energies. The measured and estimated decay properties of nuclei produced in these experiments are presented in Table 5. Estimated radioactive properties of isotopes with $Z = 112$, 114 and 116 are in good agreement to data, as we can see in Fig. 3–6, and differ from those of micro-macroscopic model calculations [21–24] (see Fig. 7).

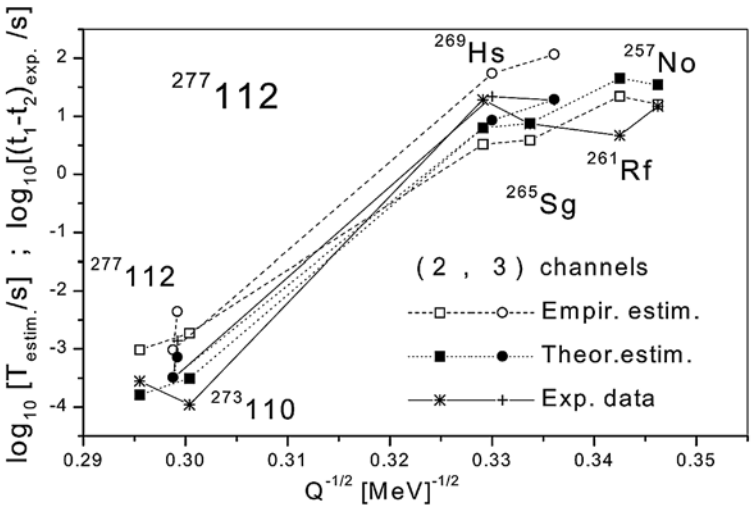

Fig. 7 – Same as in Fig. 3, but for $^{277}112$. The data are taken from [39].

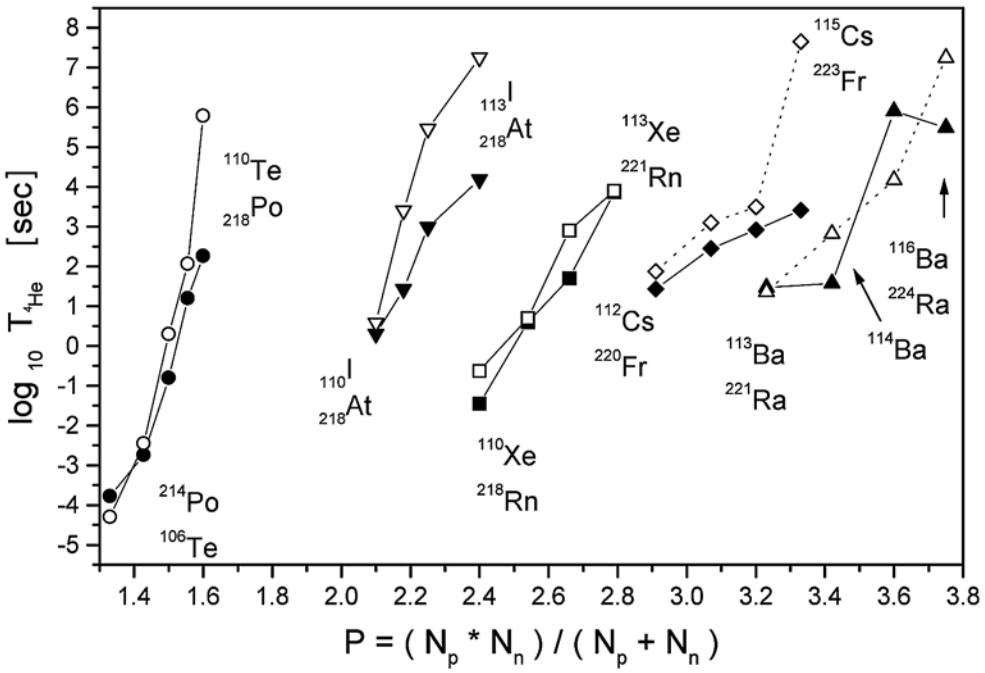

Fig. 8 – The experimental α-half-lives of *trans*-tin (open symbols) and *trans*-lead (full symbols) nuclei *versus* Casten factor $P = N_p * N_n/(N_p + N_n)$. The present calculated half-lives for Cs and Ba isotopes are connected by dot lines.

5.7. COMPARISON TO DATA AND OTHER RESULTS

The calculated half-life and some associed energy release fo "escape" particles with respect g.s.-g.s. alfa decay are shown in Tables 1–5 and Figs. 1–10, respectively. One can compare directly our results with data and some results of other models [21–28]. The usefulness of our results presented for all radioactive applications is closely connected to how our model behaves when applied to nuclei far from stability. Our results are independent on free parameters of the theory or model parameters in contrast with results of other models those parameters are used outside the region where the model parameters were determined [24].

6. DECAY PROPERTIES NEAR THE CLOSED SHELLS

6.1. α-DECAY AND CARBON EMISSION

Fig. 10 shows the released energies in isotopic sequences of the homologues from the same group *versus* the total number $N_p + N_n$ of valence nucleons. As we can see the released energy decrease with $N_p + N_n$ increasing. The neutron addition in all isotopic sequences leads to a linear decrease of energy while, the proton addition increases the emission energy. Similar trends of energy are observed in the case of two nucleon addition.

The effect on the Q_α-value caused by the addition of α-particles to the magic cores can be also observed in Fig. 10. Clearly that, in the main channels (even Z) of the trans-tin and trans-lead regions: $^{222}\mathrm{Ra} \rightarrow {}^{218}\mathrm{Rn} \rightarrow {}^{214}\mathrm{Po} \rightarrow {}^{210}\mathrm{Pb}$ and $^{114}\mathrm{Ba} \rightarrow {}^{110}\mathrm{Xe} \rightarrow {}^{106}\mathrm{Te} \rightarrow {}^{102}\mathrm{Sn}$, the Q_α-value increases when approaching the lead and tin shell closures, while in the parallel channel from the SHE region, $^{312}120 \rightarrow {}^{308}118 \rightarrow {}^{304}116 \rightarrow {}^{300}114$, the Q_α-value decreases towards the $^{298}114$ magic core. Or, such a trend of the energy in the channel of SHE region may suggest the existence of the shell closures at large values of $N_p + N_n$ (not at vanishing $N_p + N_n$ and at $Z = 114$ and $N = 184$), *i.e.*, at $Z > 114$.

However, this somewhat surprising result may be a consequence of the systematic errors the energy predictions [24]. Note that the constant difference of about 1 MeV between the energies of isotopes of elements 117 and 118 appears unusually large in comparison with experimental differences of their homologues in lead and tin regions. Since the errors in energy predictions [12] for heaviest measured 110–112 nuclei are of 0.5–0.7 MeV, one may expect for SHE 116-120 errors at least of 1 MeV. Therefore, these predictions for SHE should be considered only as rough estimations. Although, the basic properties as the mass, position of the stabilizing spherical shell proton gap as well as the origin of spin-orbit splitting of single particle states remain yet uncertain for the SHE with very large Z [26].

Fig. 11 displays the α-half-lives *versus* the Casten factor P for the nuclei whose released energies are shown in Fig. 4. Here we can see that the single proton (neutron) addition leads to systematic decrease (increase) of half-life. But, with the increase of P that means the number of "valence" α-particles [11], the half-time increases for HE and ME and decreases slowly for SHE. Notice that the calculated half-times for all the isotopic sequences with $Z = 116–120$ range in a very narrow interval (10^{-1}–10^{-5} s). In this element region an uncertainty of ±0.5 MeV in Q_α corresponds to an uncertainty in calculated T of a factor of $10^{\pm 3}$. Therefore, there are only "apparent" discrepancies between the half-lives of SHE and those of HE and ME that can be explained by uncertainties of about 0.5–0.7 MeV in used energies. In the limits of these uncertainties (for SHE) the half-lives for the homologues from the same group with an identical number of valence neutrons can be considered very close or even identical (for some HE and ME). In conclusion, the homologues from the groups VI–VIII and I, II with identical number of protons over the shell closures $Z = 50$, 82, and 114 , *i.e.* (Te, Po, 116), (I, At, 117), (Xe, Rn, 118), (Cs, Fr, 119), (Ba, Ra, 120) present not only similar chemical properties (see [20]) but also similar α-decay properties.

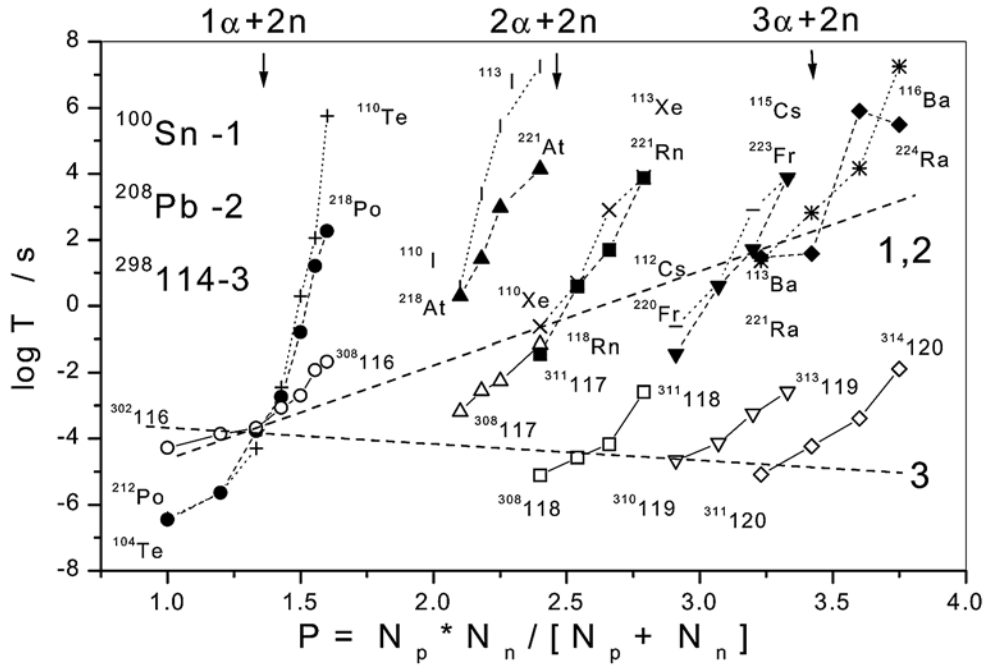

Fig. 11 – Experimental α half-lives of the trans-tin and trans-lead nuclei and calculated α half-lives for superheavy nuclei *versus* the Casten factor $P = N_p * N_n/(N_p + N_n)$. The emission energies are shown in Fig. 10.

6.2. α-DECAY PROPERTIES AND SYMMETRIES

The N_pN_n Casten-type schemes of decay properties shown in Figs. 8–11 show that the systematic evolution of basic decay properties of SHE is essentially determined by the periodic variations of the nuclear structure. Since the Q_α values (Fig. 10) appear maximized for $N_p + N_n = 4k$, $4k+2$ and $k = 1, 2, 3$ it becomes evident that maximal Q_α values and minimal half-lives T (Fig. 5) are realized by the successive addition of the α-particles and two nucleons to the double magic cores. For the decay data of the trans-led and trans-tin one may observe a clear α-periodicity and also a two periodicity. These periodicities are extended to the SHE region. First of all, the regularities in decay properties appear related to the α, ^{8}Be (2α) and ^{12}C (3α) clustering of valence nucleons. In particular, for the even Z emitters, the main α-chains corresponding to these maximal energies and minimal half-lives should be: $^{312}120 \rightarrow {}^{308}118 \rightarrow$ $\rightarrow {}^{304}116 \rightarrow {}^{300}114$, $^{222}\text{Ra} \rightarrow {}^{218}\text{Rn} \rightarrow {}^{214}\text{Po} \rightarrow {}^{210}\text{Pb}$ and $^{114}\text{Ba} \rightarrow {}^{110}\text{Xe} \rightarrow$ $\rightarrow {}^{106}\text{Te} \rightarrow {}^{102}\text{Sn}$. The members of these chains are typically α-type nuclei. The most probable individual entity in these nuclei is expected to be the α-cluster due to its high symmetry (space, spin-isospin) and high binding energy. This because, the wave function of α-particle is symmetric in the space part and antisymmetric in the spin-isospin part. Therefore, the α-decay characteristics can be understood and interpreted in a rather simple way, by studying the symmetries of model (nuclear) wave function in the coordinate space, rather than as a many-component mixed configuration wave function, in the vector space generated by single particle wave functions. For example, shape symmetries known in deformed nuclei refer to the shapes of density in the 3-space, where rather different shapes and intrinsic structures manifest themselves by regularities in energy spectra, transitions and rates [46]. Zamfir *et al.* [47–48] showed that a number of spectroscopic observables for SHE lie along smooth curves when plotted against the valence protons and neutrons, $N_p\ N_n$. Our analysis of decay properties in various schemes of the numbers of valence nucleons leads us to very similar conclusions.

Finally, it should be stressed that the fourfold magic character of the systems ($\alpha + (^{110}\text{Sn}, ^{208}\text{Pb}, ^{298}114)$) manifests through exceptionally large emission energies and rates and indicates not only the influence and importance of magicity for the decay channels but also of the high symmetry in the formation and transmission mechanisms. The fourfold magicity manifests also in production mechanism based on reactions using ($^{16}\text{O} + {}^{208}\text{Pb}$) or ($^{48}\text{Ca} + {}^{208}\text{Pb}$) that have exceptionally high cross sections.

7. CONCLUDING REMARKS

Summarizing we can conclude that the α-emission is the dominant decay mode for SHE with $102 \le Z \le 120$. Characteristic for these nuclides are very long α-chains as well as parallel sequences of or α-decays terminated by spontaneous fission. The long α-half-lives of the these nuclei allow the application of the methods of α-spectroscopy, giving new information about nuclear and atomic properties of the heaviest elements. In most cases our α-halftime estimates are in excellent agreement to existing data. Such an agreement supports the basic correctness of our unified picture for heavy-ion and α resonances giving us guaranties for reliable predictions for more heavier elements under the current research. The study of nuclei passing from spherical to deformed shapes in the course of their consecutive α-decays provides valuable information about the influence of significant structure changes on the nuclear decay properties properties of SHE.

Experimentally, there is a clear evidence for clustering and fine structure in SHE. The capabilities for investigating these typical structures in SHE have been extended by the development of the techniques of resonant-particle spectroscopy and the employment of the recoil decay tagging method in connection to in-beam measurements. More detailed spectroscopic measurements will be required to understand typical structures in SHE. Clustering and "fine structure" studies allow to reveal the information on the decaying system, the initial correlations in the reacting nuclei as well as to yield spectroscopic informations on the continuum states populated in in the unbound intermediate systems in the decay channel. We may expect as a general rule that clusterisation and formation of long α-chains will occur for SHE close to the threshold to α-particle substructures. The formation of such structures via condensation from a nuclear medium consisting of α-particles and neutrons may be expected to occur, the formation of chain radioactive states can possibly be observed in various central nuclear collisions. The unambiguous identification of new SHE and study of their basic properties will need still experimental and theoretical efforts.

We get that the homologues elements from the same groups VI–VIII and I, II of the Periodic Table with identical numbers of valence protons and neutrons above the doubly magic closures $^{298}114$, $^{208}Pb_{82}$ and $^{100}Sn_{50}$ exhibit almost identical or similar α-decay properties. Therefore, from what we know in the ^{208}Pb and ^{100}Sn regions and using the arguments of symmetry it was possible to make reliable extrapolations for the region of SHE. We have proven the utility of Casten-Zamfir type schemes and α-cluster model in study the structure and decay properties of spherical and deformed nuclei. Another important conclusion is that the α-clustering and deformations appear intrinsically connected through the number of valence nucleons and their two-body interactions. Nevertheless, parallel extra-

polations of nuclear decay properties and chemical properties that exploit the fundamental relationships of the physicochemical data that exist in the groups and periods of the Periodic Table offer us a very solid basis for interpretation of experimental results. We wish to emphasize that the evidence on radioactive states in SHE, resonance phenomena in reaction with ion beams and macroscopic decay properties obtained by the approaches used at present time cannot be perfect, because it is inherently indirect. Still one can gradually approach the goal by accumulating diverse data, improving statistics, extending systematics of basic properties at the limits, and developing underlying theories. Its especially important to stand the temptation of making conclusions which would go beyond the experimental data and their accuracy. These general problems and concerns are fully applicable to fusion-decay studies. Based on the measured production cross sections of new nuclides, their synthesis in the cross bombardments, as well as comparison of their decay properties with experimental systematics and theoretical predictions, is is most reasonable to assign observed nuclei to the products of the complete fussion reactions followed by neutron evaporation.

Acknowledgments. We thank S. Hofmann, G. Münzenberg, Yu. Ts. Oganessian, V. K. Utynkov, V. Voronov, and A. Nasirov for many stimulating discussions. This work was supported in part from Contracts IFA-IFIN-HH: CERES-3/40,41and 4/218.

REFERENCES

1. T. Teichmann, E. P. Wigner, Phys. Rev., 79, 30 (1952).
2. R. G. Thomas, Prog. Theor. Phys., 12, 253 (1954).
3. H. J. Mang, Phys. Rev., 119, 1069 (1960).
4. H. J. Mang, J. O. Rasmussen, Kgl. Danske Videnscab Selskab, Mat.-Fys. Skifter 2, (1962) No. 3.
5. H. J. Mang, Ann. Rev. Nucl. Sci., 14 (1984).
6. G. Breit, Encyclopedia of Physics, Vol. XLI, Nuclear Reactions II: Theory, Springer-Verlag, 1959, (ed. S. Flugge).
7. H. Feshbach, Ann. Phys. 5 (NY), 357 (1958).
8. K. Harada, E. A. Rauscher, Phys. Rev., 169, 818 (1968).
9. S. G. Kadmensky, V. E. Kaletchits, Yad. Fiz., 12, 70 (1970).
10. J. Schlitter, Nucl. Phys., A 211, 96 (1973).
11. D. F. Jakson , M. Roades-Brown, Ann. Phys., 105 (NY), 151 (1977).
12. A. Sandulescu, I. Silisteanu, R. Wuensch, Nucl. Phys., A305, 205 (1978).
13. K. Wildermuth, Y. C. Tang, F. Fernandez, E. J. Kanellopoulos, W. Sunkel, J. Phys., G6, 603 (1980).
14. Phys. Rep. 294, 265 (1998), R. G. Lovas, R. J. Liotta, A. Insolia, K. Varga, DS. Delion.
15. I. Rotter, Rep. Prog. Phys., 54, 635 (1991).
16. W. Greiner, J. Y. Park and W. Scheid, in Nuclear Molecules, World Scientific (Songapore-New Jersey-London-Hong Kong, 1995), Chap. (5-7).
17. I. Silişteanu, W. Scheid, Phys., Rev. C 51, 2023 (1995).
18. I. Silişteanu , W. Scheid and A. Sandulescu, Nucl. Phys, A 679, 317 (2001).
19. M. Ivascu, I. Silisteanu, Nucl. Phys., A 485, 93 (1988).
20. M. Ivascu, I. Silisteanu, Sov. J. Part. Nucl., 21, 599 (1990).
21. V. E. Viola and G. T. Seaborg, J. Inorg. Nucl. Chem., 28, 741 (1966).

22. A. Sobiczewsky, Z. Patyk, and S Cwiok, Phys. Lett., B 224, 1 (1989).
23. Z. Patyk and A. Sobiczewski, Nucl. Phys., A354, 229 (1996).
24. P. Möller, R. J. Nix and K. L. Kratz, At. Data and Nucl. Data Tab. 66, 131 (1997).
25. B. A. Brown, Phys. ReV., 58, 220 (1998).
26. K. Rutz, M. Bender, T. Burvenich, T. Schilling, P.-G. Reinhardt, J. A. Maruhn, W. Greiner, Phys. Rev., C 56, 238 (1997).
27. S. Goliely, F. Tondeur, J. M. Pearson, At. Data Nucl. Data Tables, 77, 311 (2001).
28. S. K. Patra, Cheng-Li Wu, W. Greiner and Raj K. Gupta, J. Phys. G: Nucl. Part. Phys., 26, 1569 (2000).
29. D. S. Delion, A. Insolia, R. J. Liotta, Phys. Rev., C54, 292 (1996).
30. R. Blendovske, T. Fliessbach, H. Walliser, Z. Phys., A339, 121 (1991).
31. M. Grigorescu,B. A. Brown, O. Dumutrescu, Phys. Rev., C47, 2666 (1993).
32. A. Bulgac, S. Holan, F. Carstoiu, O. Dumitrescu, Nuovo Cimento, 70 A, 142 (1982).
33. I. Silisteanu, M. Ivascu, J. Phys. G: Nucl. Part. Phys., 15, 1405 (1990).
34. D. Robson, Nucl. Phys., A 204, 204 (1973).
35. B. R.Fulton and W. D. M. Rae, J. Part. Phys., 16, 333 (1990).
36. R. S. Simon *et al.*, Z. Phys., A325, 197 (1986).
37. S. Hofmann, N. Ninov, F. P. Hesberger, P. Ambruster, H. Folger, G. Münzenberg, H. J. Schott, A. G. Popeko, A. V. Yeremin, A. N. Andreyev, S. Saro, R. Janik, M. Leino, Zeits. Physik, A 350, 281 (1995).
38. S. Hofmann, N. Ninov, F. P. Hesberger, P. Ambruster, H. Folger, G. Münzenberg, H. J. Schott, A. G. Popeko, A. V. Yeremin, A. N. Andreyev, S. Saro, R. Janik, M. Leino, Zeits. Physik, A 354, 229 (1996).
39. S. Hofmann and G. Münzenberg, Rev. Mod. Phys., 72, 733 (2000).
40. Yu. Ts. Oganessian, V. K. Utynkov, Yu. V. Lobanov, F. Sh Abdullin, A. N. Polyakov, I. V. Shirokovsky, Yu. S. Tsiganov, G. G. Gulbekian, S. L. Bogomolov, B. N. Gikal, A. N. Mezentsev, S. Iliev, V. G. Subbotin, A. M. Sukhov, G. V. Buklanov, K. Subotic, M. G. Itkis, K. J. Moody, J. F. Wild, M. A. Stoyer, R. W. Lougheed, Phys. Rev. Lett., 83, 3154 (1999).
41. Yu. Ts. Oganessian, A. V. Yeremin, A. G. Popeko *et al.*, Nature (London), 400, 242 (1999).
42. Yu. Ts. Oganessian, V. K. Utynkov, Yu. V. Lobanov, F. Sh Abdullin, A. N. Polyakov, I. V. Shirokovsky, Yu. S. Tsiganov, G. G. Gulbekian, S. L. Bogomolov, B. N. Gikal, A. N. Mezentsev, S. Iliev, V. G. Subbotin, A. M. Sukhov, G. V. Buklanov, K. Subotic, M. G. Itkis, K. J. Moody, J. F. Wild, M. A. Stoyer, R. W. Lougheed, Phys. Rev., C 62, 041604 (R) (2000).
43. Yu. Ts. Oganessian, V. K. Utynkov, Yu. V. Lobanov, F. Sh Abdullin, A. N. Polyakov, I. V. Shirokovsky, Yu. S. Tsiganov, G. G. Gulbekian, S. L. Bogomolov, B. N. Gikal, A. N. Mezentsev, S. Iliev, V. G. Subbotin, A. M. Sukhov, O. V. Ivanov, G. V. Buklanov, K. Subotic, M. G. Itkis, K. J. Moody, J. F. Wild, M. A. Stoyer, R. W. Lougheed, Phys. Rev., C 62, 011301 (R) (2000).
44. Yu. Ts. Oganessian, V. K. Utynkov, Yu. V. Lobanov, F. Sh Abdullin, A. N. Polyakov, I. V. Shirokovsky, Yu. S. Tsiganov, G. G. Gulbekian, S. L. Bogomolov, B. N. Gikal, A. N. Mezentsev, S. Iliev, V. G. Subbotin, A. M. Sukhov, A. M. Voinov, G. V. Buklanov, K. Subotic, M. G. Itkis, K. J. Moody, J. F. Wild, M. A. Stoyer, N. J. Stoyer, D. A. Shughnessy, J. M. Kenneally, R. W. Lougheed, C. A. Laue, Ye. A. Karelin, A. N. Tatarinov, Phys. Rev., C.69, 021601 (2004).
45. Yu. Ts. Oganessian, V. K. Utynkov, Yu. V. Lobanov, F. Sh Abdullin, A. N. Polyakov, I. V. Shirokovsky, Yu. S. Tsiganov, G. G. Gulbekian, S. L. Bogomolov, B. N. Gikal, A. N. Mezentsev, S. Iliev, V. G. Subbotin, A. M. Sukhov, A. M. Voinov, G. V. Buklanov, K. Subotic, V. I. Zagrebaev, M. G. Itkis, J. B. Patin, K. J. Moody, J. F. Wild, M. A. Stoyer, M. AQ. Stoyer, R. W. Lougheed, Phys. Rev., C.69, 054607 (2004).
46. S. Cwiok, W. Nazarewicz and P. H. Heenen, Phys. Rev. Lett., 83, 1108 (1999).
47. N. V. Zamfir, G. Hering, R. F. Casten and P. Paul, Phys. Lett. B, 357, 515 (1995).
48. N. V. Zamfir, Private Communication, (2005).

8. APPENDIX

8.1. EQUATIONS OF MOTION

Let us consider the case when exist appreciable interactions between the emitted particle waves with different final states of the deformed daughter nucleus. The Hamiltonian of the system is written as:

$$H = -\frac{\hbar^2}{2m}\nabla^2 + H_p + H_D + \hat{V}(r) \tag{22}$$

where $T_r = -\frac{\hbar^2}{2m}\nabla^2$ is the kinetic energy operator for the relative motion, $\hat{V}(r)$ is the potential energy operator

$$\hat{V}(r) = V^{nucl.}(r) + V^{Coul.}(r) + V^{so}(r) + V^{cent.}(r) \tag{23}$$

those components are parametrized in Appendix. The Hamiltonians of the fragments H_D and H_p satisfy the Schrodinger equations

$$H_D \left|\phi_D\right\rangle = E_D \left|\phi_D\right\rangle \tag{24}$$

$$Hp\left|\phi_p\right\rangle = H_p \left|\phi_p\right\rangle. \tag{25}$$

The Hamiltonian (16) describes the scattering states

$$\left|\chi_{nE}\right\rangle = \left[\left|\phi_D\right\rangle\left|\phi_p\right\rangle\left|lm\right\rangle\left|u_{Ql}\right\rangle\right]_n \tag{26}$$

which consist of products of intrinsic states of the daughter nucleus $\left|\phi_D\right\rangle$, emitted particle $\left|\phi_p\right\rangle$ and also the angular parts $\left|u_{Ql}\right\rangle$ of the relative motion characterized by the angular momentum l and projection m and the energy Q of the relative motion. In () n denotes a channel index.

The WF $\left|\phi_D\right\rangle$ is assumed of the form:

$$\left|\Phi_D\right\rangle = \left|\phi_D^{Rm_R}\right\rangle = [(2R+1)/8\pi^2]D^{R*}_{m_R 0}(\alpha\beta\gamma)\phi_D^{int.}(\eta_1) \tag{27}$$

where and the phase convention:

$$D^R_{m_R 0}(\alpha\beta\gamma) = [4\pi/(2R+1)]Y_R^{m_R *}(\beta\alpha) \tag{28}$$

where $\phi_D^{int.}(\eta_1)$ is the internal w.f. of coordinates η_1, R is the total spin of the daughter nucleus and its projection is m_R. The WF $\left|\phi_p\right\rangle$ is the product of the space and spin components:

$$\left|\Phi_p\right\rangle = \phi_p^{int\cdot}(\eta_2)\sigma_{sm_s} \tag{29}$$

With (27) and (29) we rewrite the total scattering wave function of the system as follows:

$$\left|\chi_{nE}\right\rangle = \sum_{IM} \chi_E^{IM}(r, \eta_1, \eta_2) = \sum_{IM} \frac{1}{r} \sum_{Rjl} u_{IRjl}(r)\Phi_{Rjl}^{IM}(\hat{r}, \eta_1, \eta_2) \tag{30}$$

where the angular momentum-spin WF of the channel $\left|n\right\rangle$ is given by

$$\Phi_{Rjl}^{IM}(\hat{r}, \eta_1, \eta_2) = \sum_{m_R m_l m_s} C_{m_l m_R M}^{lRI} C_{m_l m_s m}^{lsj} \Phi_D^{Rm_R}(\eta_1)\{\phi_p^{int\cdot}(\eta_2) i^l Y_{lm_l}(\hat{r})\sigma_{sm_s}\}, \tag{31}$$

the channel index being denoted by $n = \{I, R, l\}$.

The space formed by scattering states $\left|\chi_{nE}\right\rangle$ with $Q > 0$ will be denoted by P-space, while the space of bound states $\left|\phi_k\right\rangle$ is denoted by Q. Both scattering and bound states are normalized

$$\left\langle\chi_{nE}\middle|\chi_{nE'}\right\rangle = \delta_{nn'}\delta(E - E'); \quad \sum_k \left\langle\phi_k\middle|\phi_{k'}\right\rangle = \delta_{kk'}, \tag{32}$$

so that we can define the projection operators:

$$P = \sum_n \int dE \left|\chi_E^n\right\rangle\left\langle\chi_{E'}^n\right|; \qquad Q = \sum_k \left|\phi_k\right\rangle\left\langle\phi_{k'}\right| \tag{33}$$

If there are no other open channels, P and Q determine two orthogonal subspaces of functional space of decaying nucleus and their sum is a complete functional space of the whole system:

$$PQ = QP = 0; \quad P + Q = 1 \tag{34}$$

States $\left|\phi_k\right\rangle$ and $\left|\chi_E^n\right\rangle$ are eigenstates of projected Hamiltonian in the corresponding subspaces ($H_{QQ} = QHQ$, $H_{PP} = PHP$):

$$(E - H_{PP})\left|\chi_E^n\right\rangle = 0 \tag{35}$$

$$(E_k - H_{QQ})\left|\phi_k\right\rangle = 0 \tag{36}$$

In order to satisfy (34) the scattering states must be orthogonal to the bound states:

$$\left\langle\phi_k\middle|\chi_E^n\right\rangle = 0. \tag{37}$$

Thus eigenstates of the total Hamiltonian (written as a sum over two components $|\Psi\rangle = P|\Psi\rangle + Q|\Psi\rangle$) are obtained from:

$$(E-H)|\Psi\rangle = 0, \tag{38}$$

While the bound states $|\phi_k\rangle$ can be obtained by diagonalizing a shell model Hamiltonian in a truncated space (Eq. ()), we have still to calculate scattering states from Eq. () using Eq. ():

$$(E-H)|\chi_{nE}\rangle = -QH|\chi^n_{nE}\rangle = -\sum_k \langle\phi_{k'}|H|\chi^n_E\rangle|\phi_k\rangle \tag{39}$$

i.e., an integral equation.

Denoting by $|\chi^0_{nE}\rangle$, the solution of the homogeneous equation which fulfils the usual boundary conditions for scattering states (incoming waves in the channel and outgoing waves in all open channels)

$$(E-H)|\chi^0_{nE}\rangle = 0, \tag{40}$$

and by $|\chi^k_{nE}\rangle$ the solution of inhomogeneous equation

$$(E-H)|\chi^k_{nE}\rangle = |\phi_k\rangle \tag{41}$$

which vanishes at large separations, the solution of eq. (39) can be written as

$$|\chi_{nE}\rangle = |\chi^0_{nE}\rangle - \sum_k \langle\phi_{k'}|H|\chi^n_E\rangle|\chi^k_{nE}\rangle \tag{42}$$

$$\Gamma^k = 2\pi\sum_n |\langle\phi_k|H|\chi^n_E\rangle|^2 = 2\pi\sum_n \left|\frac{\langle\phi_k|\chi^0_E\rangle}{\langle\phi_k|\chi^k_E\rangle}\right|^2. \tag{43}$$

8.2. INTERACTION POTENTIAL

8.2.1. Spherical system

The Woods-Saxon parametrization is used for the nuclear potential in Eq. (5)

$$V^{nucl.}(r) = -V_0 f(r, a, R_0) + iWg(r, b, R_0). \tag{44}$$

$$f(r, a, R_0) = -V_0/(1+\exp((r-R_0)/a)); \quad g(r, b, R_0) = 4\exp(r-R_0)/af^2(r, b, R_0) \tag{45}$$

with $R_0 = r_0(A_D^{1/3} + A_p^{1/3})$ and a and b are diffuseness parameters.

The Coulomb potential is taken of the form:

$$V^{Coul.}(r, R_c) = \left\{ \begin{array}{c} \dfrac{Z_p Z_D^2 e^2}{R_c}\left[3 - \left(r/R_c\right)^2\right] r \le R_c \\ \dfrac{Z_p Z_D^2 e^2}{R_c} r \ge R_c \end{array} \right\}; \quad R_c = r_c(A_D^{1/3} + A_p^{1/3}) \qquad (46)$$

The spin-orbit part of the potential is

$$V^{so}(r) = 2(\hbar/m_\pi c)^2 D^{so} \frac{1}{r} \frac{\mathrm{d}f(r, a_{so}, R_{so})}{\mathrm{d}r}(l * s) \qquad (47)$$

where D^{so} is the spin-orbit depth.

8.2.2. Deformed system

The above parametrization are adopted for the deformed potential.

The nuclear Hamiltonian can be generated by changing the radius of the daughter nucleus in ( ) to a dynamical operator

$$R_0 \to R_0 + \hat{O} = R_0 + \beta_2 R_D Y_{20} + \beta_4 R_D Y_{40} \qquad (48)$$

where β_2 and β_4 are the quadrupole and hexadecapole deformation parameters of the ( ) deformed daughter nucleus, respectively.

The nuclear formfactor in ( ) is thus given by

$$f(r, \hat{O}) = -V_0/(1 + \exp((r - R_0 - \hat{O})/a) \qquad (49)$$

TheCoulomb Hamiltonian can be generated by changing the radius of the daughter nucleus in ( ) to a dynamical operator

$$R_c \to R_c + \hat{O} = R_c + \beta_2 R_D Y_{20} + \beta_4 R_D Y_{40} \qquad (50)$$

8.2.3. Coupling interaction

In order to obtain the nuclear and nuclear coupling Hamiltonians we first look for the eigenvalues and eigenvectors of the operator $\hat{O}$ which satisfies:

$$\hat{O}|\alpha\rangle = \lambda_\alpha |\alpha\rangle. \qquad (51)$$

The matrix elements of nuclear coupling Hamiltonian between the $|n\rangle = |I'0\rangle$ and $|m\rangle = |I'0\rangle$ states of the ground rotational band of the daughter are obtained by diagonalizing the matrix $\hat{O}$:

$$\hat{O}_{II'} = \left[\frac{5(2I+1)(2I'+1)}{4\pi}\right]^{1/2} \beta_2 R_D \begin{pmatrix} I & 2 & I' \\ 0 & 0 & 0 \end{pmatrix}^2 \qquad (52)$$

$$+\left[\frac{9(2I+1)(2I'+1)}{4\pi}\right]^{1/2}\beta_4 R_D\begin{pmatrix} I & 4 & I' \\ 0 & 0 & 0 \end{pmatrix}^2 \tag{53}$$

Then, the nuclear coupling martrix elements are given by

$$\begin{aligned} V_{nm}^{nucl.}(r) &= \langle I0|V^{nucl.}(r,\hat{O})|I'0\rangle - \delta_{nm}V_0^{nucl.}(r) = \\ &= \sum_{\alpha}\langle I0|\alpha\rangle\langle\alpha||I'0\rangle V^{nucl.}(r,\lambda_\alpha) - \delta_{nm}V_0^{nucl.}(r) \end{aligned} \tag{54}$$

last term in this equation is included to avoid the double counting of the diagonal component.

Similarly, the Coulomb matrix elements are then given by

$$\begin{aligned} V_{nm}^{Coul.}(r) = {} & \frac{3Z_D Z_p R_D^2}{5r^3}\left[\frac{5(2I+1)(2I'+1)}{4\pi}\right]^{1/2}\left(\beta_2 + \frac{2}{7}(5/\pi)^{1/2}\beta_2^2\right)\begin{pmatrix} I & 2 & I' \\ 0 & 0 & 0 \end{pmatrix}^2 + \\ & + \frac{3Z_D Z_p R_D^2}{9r^5}\left[\frac{9(2I+1)(2I'+1)}{4\pi}\right]^{1/2}\left(\beta_4 + \frac{9}{7}\beta_2^2\right)\begin{pmatrix} I & 4 & I' \\ 0 & 0 & 0 \end{pmatrix}^2. \end{aligned} \tag{55}$$

Table 5

Experimental and estimated decay properties of nuclei produced by Yu. Ts. Oganessian *et al.* [45], Phys. Rev. C 69, 054607 (2004)

Nuclide	No. observed events	Decay mode	Half-life Exp.	Expected half-life Exp.	E_α [MeV] Exp.	Half-life Theor.	Expected half-life Theor.
$^{293}116$	3	α	53^{+62}_{-19} ms	80 ms	10.53 ± 0.06	71^{+31}_{-22} ms	71 ms
$^{289}114$	8	α	$2.7^{+1.4}_{-0.7}$ s	2.0 s	9.82 ± 0.06	$2.29^{+1.4}_{-0.7}$ s	2.29 s
$^{285}112$	8	α	34^{+17}_{-9} s	50.0 s	9.16 ± 0.06	77.3^{+43}_{-27} s	77.3 s
$^{281}110$	8	SF	$9.6^{+5.0}_{-2.5}$ s				
$^{288}114$	11	α	$0.63^{+0.28}_{-0.14}$ s	0.80 s	9.95 ± 0.08	$1.01^{+0.7}_{-0.4}$ s	1.01 s
$^{284}112$	11	SF	98^{+41}_{-23} ms				
$^{291}116$	2	α	$6.3^{+11.6}_{-2.5}$ ms	20.00 ms	10.74 ± 0.07	22^{+11}_{-8} ms	22 ms
$^{287}114$	3	α	$1.1^{+1.3}_{-0.4}$ s	0.50 s	10.04 ± 0.07	$0.58^{+0.34}_{-0.2}$ s	0.58 s
$^{283}112$	3	α	$6.1^{+7.2}_{-2.24}$ s	3.00	9.54 ± 0.07	$5.63^{+3.52}_{-2.14}$ s	5.63 s
$^{279}110$	3	SF	$0.29^{+0.35}_{-0.10}$ s				
$^{290}116$	3	α	15^{+26}_{-6} ms	10 ms	10.85 ± 0.08	12^{+7}_{-5} ms	12 ms
$^{286}114$	2	α/SF	$0.29^{+0.54}_{-0.11}$ s	0.50 s	10.03 ± 0.31	$0.64^{+4.44}_{-0.53}$ s	0.64 s
$^{282}112$	1	SF	$1.0^{+4.8}_{-0.5}$ ms				

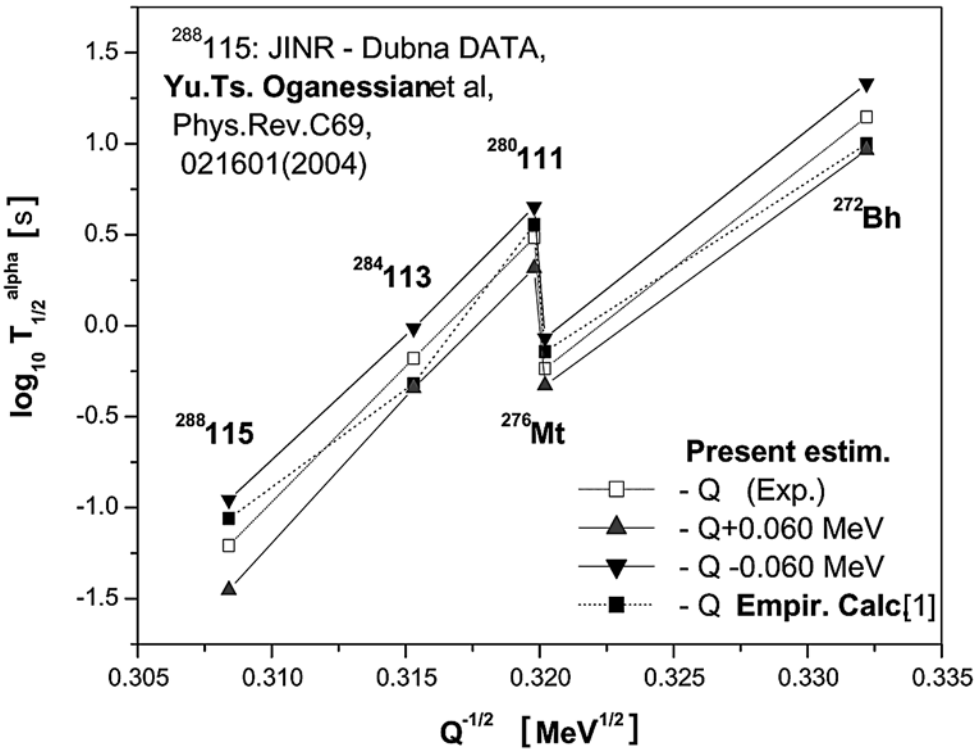

Fig. 4 – Same as in Fig. 3, but for $^{288}115$. Data and empirical calculation are taken from [44].

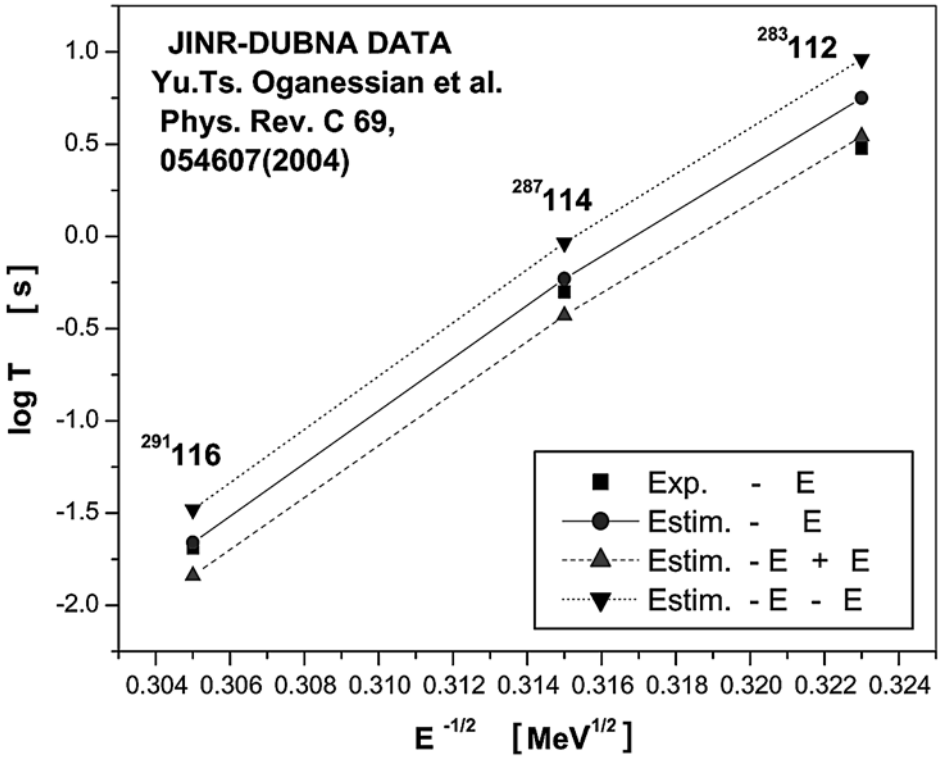

Fig. 5 – Same as in Fig. 3, but for $^{293}116$.

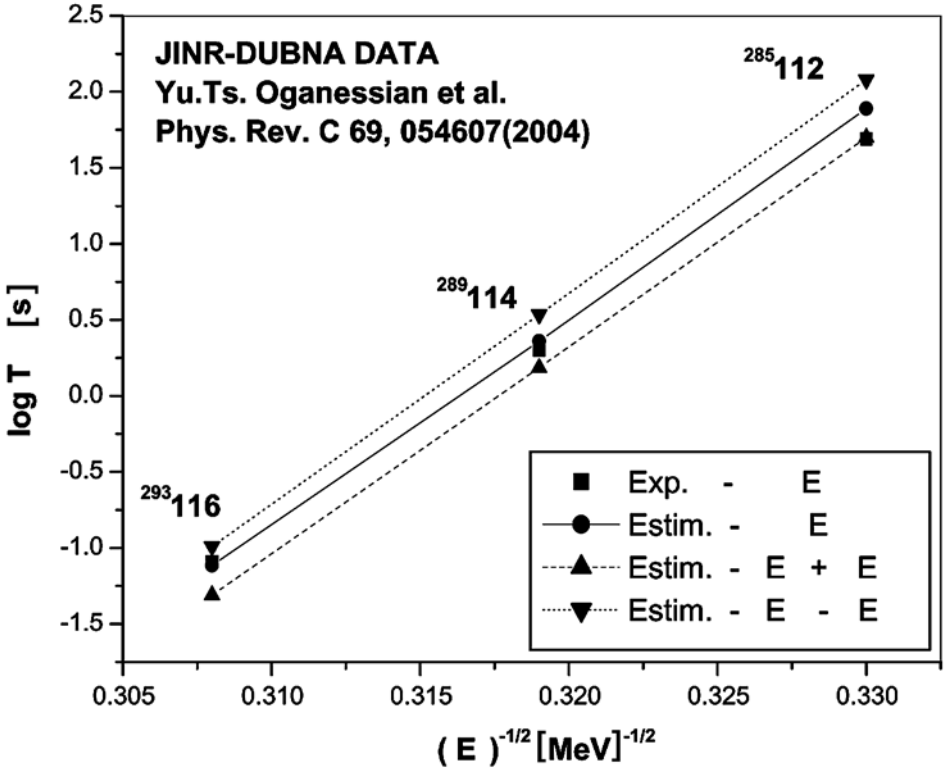

Fig. 6 – Same as in Fig. 3, but for $^{293}116$.

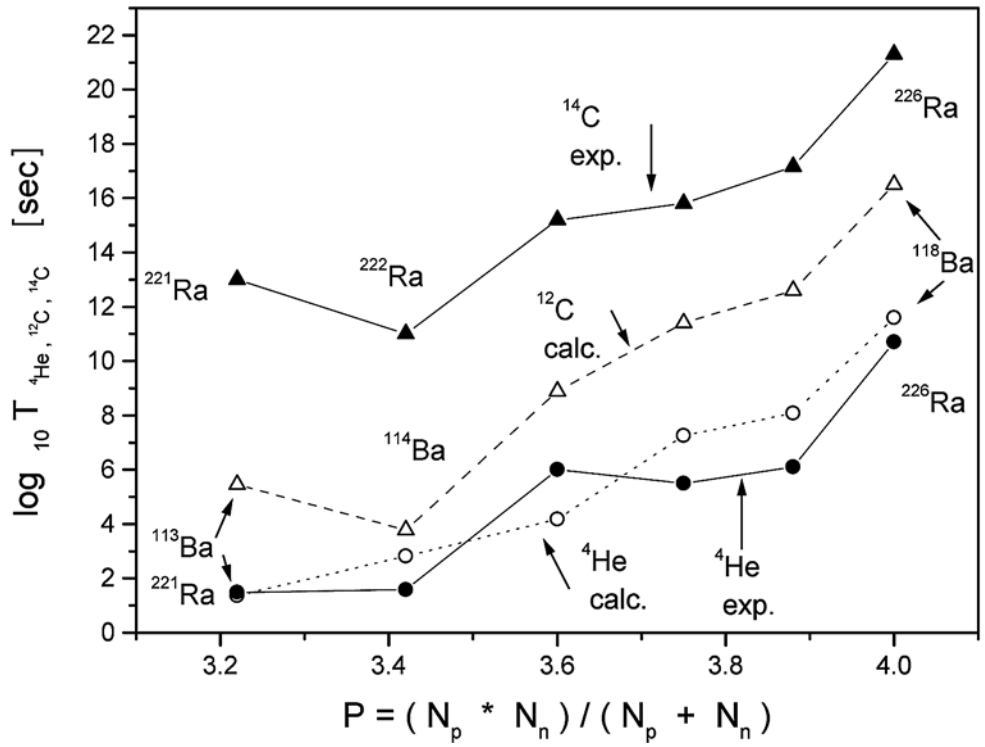

Fig. 9 – Lifetimes of α and ^{12}C emission from Ba isotopes (calculated – open symbols [12]) and of α and ^{14}C emission from Ra isotopes (experimental – full symbols) *versus* the factor $P = N_p * N_n/(N_p + N_n)$.

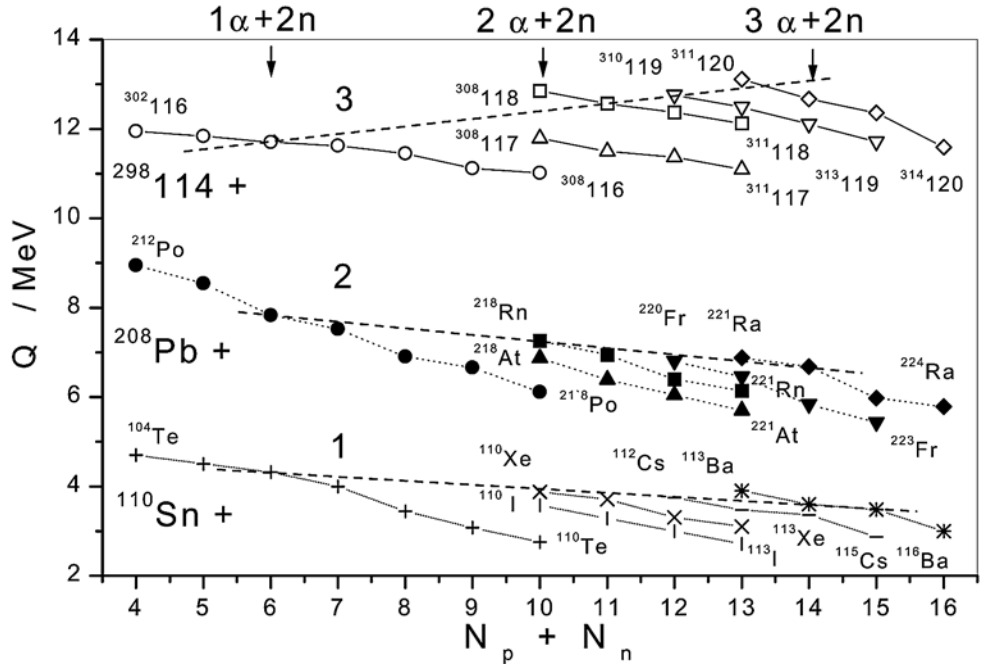

Fig. 10 – Emission energies of some SHE, HE and *trans*-tin elements *versus* the total number of valence nucleons $N_p + N_n$ above the double shell closures ^{100}Sn ^{208}Pb and ^{298}114. Calculated values (open symbols) are taken from [12] for SHE and for ^{112,115}Cs and $^{113–116}$Ba isotopes. Measured values for the *trans*-lead and *trans*-tin elements are denoted by full symbols.